

# Precise acquisition and unsupervised segmentation of multi-spectral images

David Delgado Gomez <sup>\*</sup>, Line Harder Clemmensen, Bjarne K. Ersbøll,  
Jens Michael Carstensen

*Computational Imaging Laboratory, Department of Technology, Universitat Pompeu Fabra, Pg. de Circumval.lacio 8, Barcelona 08003, Spain*  
*Informatics and Mathematical Modelling, Technical University of Denmark, Building 321, DK-2800 Lyngby, Denmark*

Received 5 December 2005; accepted 15 June 2006

Available online 19 December 2006

Communicated by James Davis and Riad Hammoud

## Abstract

In this work, an integrated imaging system to obtain accurate and reproducible multi-spectral images and a novel multi-spectral image segmentation algorithm are proposed. The system collects up to 20 different spectral bands within a range that vary from 395 nm to 970 nm. The system is designed to acquire geometrically and chromatically corrected images in homogeneous and diffuse illumination, so images can be compared over time. The proposed segmentation algorithm combines the information provided by all the spectral bands to segment the different regions of interest. Three experiments are conducted to show the ability of the system to acquire highly precise, reproducible and standardized multi-spectral images and to show its applicabilities in different situations.

© 2006 Elsevier Inc. All rights reserved.

*Keywords:* Image acquisition; Multi-spectral image analysis; Illumination; Exploratory data analysis; Image segmentation; Pattern recognition

## 1. Introduction

According to Wyszecky [1], color is defined as the aspect of visual perception by which an observer may distinguish differences between two structure-free fields of view of the same size and shape. Since the beginning of image analysis, several color models have been developed with the goal of enhancing the contrast of the different structures embedded. These color spaces have made the segmentation of the interesting structures easier in several problems. For instance, two of these color spaces, the CIE-XYZ and the CIE- $L^*a^*b^*$  [1] have been successfully applied to the segmentation of dermatological lesions [2,3]. These two color

spaces are frequently used in Dermatology because of the uniformity of the CIE- $L^*a^*b^*$  color space. This uniformity that helps to understand how different two colors will look to a human observer is directly connected with dermatologist's visual lesion evaluation. These two color spaces are, respectively, a linear and a non-linear transformation of the RGB color space.

Other color spaces have also been developed aiming at enhancing the interesting structures in other image analysis areas. For example, the YCbCr color space has been widely applied in facial and skin detection [4,5], the HSV color space in food assessment and fungi detection [6,7], and the CIE- $L^*u^*v^*$  color space in diabetes and retinopathy detection [8,9]. However, the appearance of new multi-spectral equipments that capture more than just the tri-chromatic bands, the need of finding new transformations that include the information provided by the new bands has emerged.

<sup>\*</sup> Corresponding author.

*E-mail addresses:* [david.delgado@upf.edu](mailto:david.delgado@upf.edu) (D.D. Gomez), [lhc@imm.dtu.dk](mailto:lhc@imm.dtu.dk) (L.H. Clemmensen), [be@imm.dtu.dk](mailto:be@imm.dtu.dk) (B.K. Ersbøll), [jmc@imm.dtu.dk](mailto:jmc@imm.dtu.dk) (J.M. Carstensen).

A tool that has been considered to overcome this problem is principal component analysis (PCA) [10]. This multivariate statistical technique consists of an eigenvalue analysis of the covariance matrix for a multidimensional stochastic variable. Given a random  $n$ -dimensional variable, the  $i$ th principal component is the linear combination, with normed coefficients, of the original variables which is uncorrelated with the  $i - 1$  first principal components and it has the largest variance. This  $i$ th principal component corresponds to the eigenvector associated with the  $i$ th largest eigenvalue of the covariance matrix. In many cases, the first few PCs explain most of the variance in data and can therefore often enhance the desired structures.

However, although this technique has successfully been applied in some data reduction and classification problems [11,12], it is not able to provide a suitable solution in other classification problems. An example of this is illustrated applying PCA to the dataset displayed in Fig. 1(a). This synthetic dataset was generated according to a mixture of two Gaussian populations with 20,000 and 10,000 data points, means  $[0,0]$  and  $[0,10]$ , and covariance matrices

$$\begin{pmatrix} 9 & 9 \\ 9 & 10 \end{pmatrix} \text{ and } \begin{pmatrix} 1 & 0 \\ 0 & 25 \end{pmatrix},$$

respectively. The two principal components obtained are shown in Fig. 1(b) and (c). Note, that none of the two principal components are able to separate the Gaussian populations. Moreover, it is shown in Fig. 1(d) that it is possible to find a bimodal one-dimensional projection that separates both populations. Therefore, there exists a need to find an optimal projection from a classification point of view that enhances the different structures in the image.

This need is added to the already existing challenge of collecting precise and reproducible images so images collected at different times can precisely be compared. Different research projects in color calibration [13] and illumination control [14] have been developed with the goal of achieving these two goals. The consequence of these studies is the appearance of new equipments which aims at obtaining precise images within the last years. For instance, in dermatology, Magliogiannis [15] developed a system that aimed at reducing the shadows produced by the human body curvature. However, as it was shown by Gutenev et al. [16], there are at least two current problems in the acquisition of the images: specular reflection and misalignments. Lack of precision in the image acquisition has been prevented using suitable methods to objectively evaluate the images.

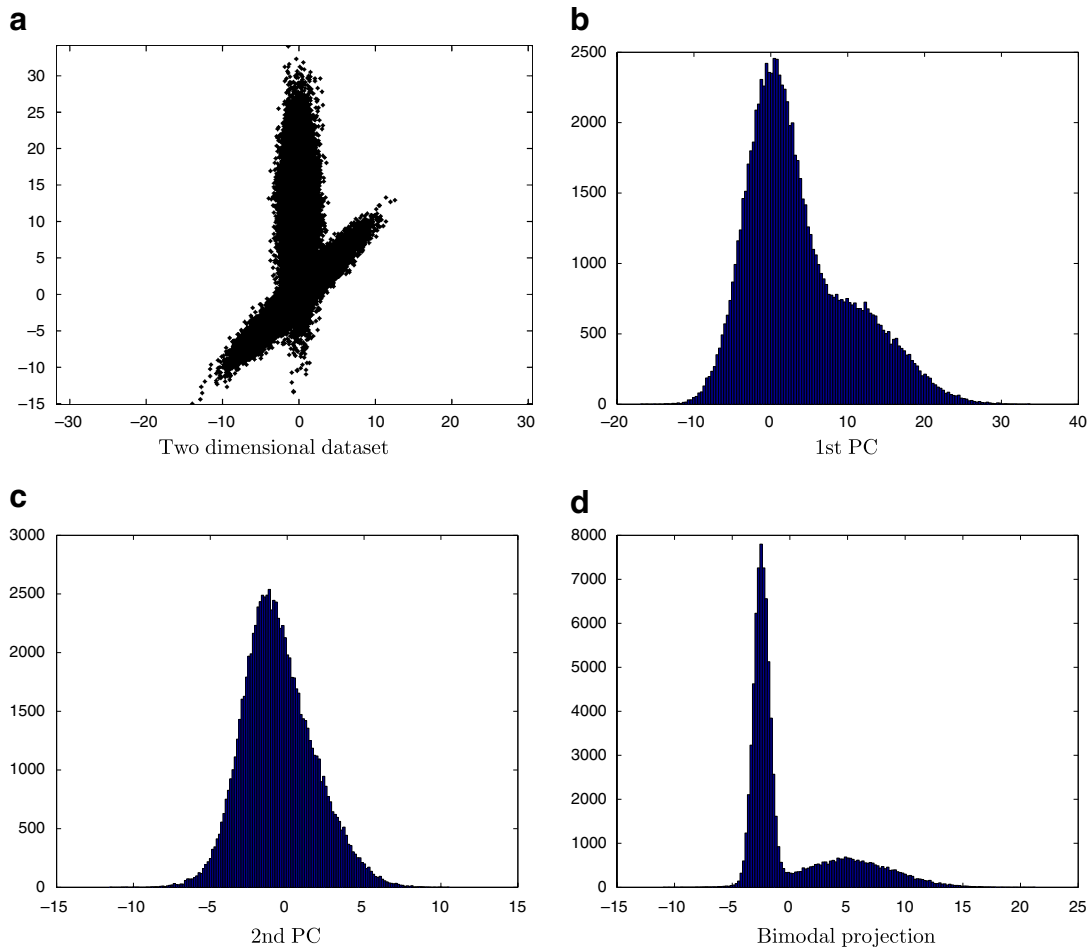


Fig. 1. A two-dimensional dataset, its two principal components (PC) and a bimodal projection of the dataset.

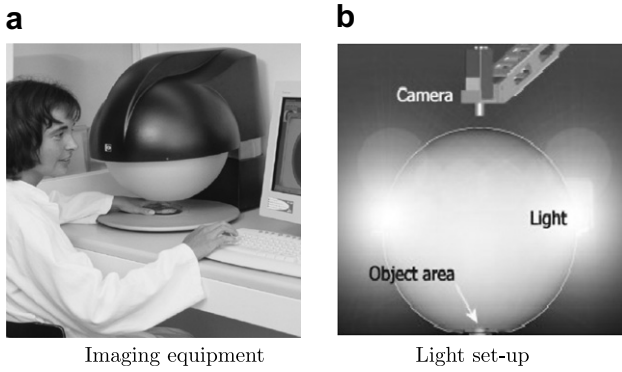


Fig. 2. The camera system.

In this work, two solutions are proposed to deal with the two situations: an imaging system to collect precise and reproducible images and an algorithm to find suitable projections which easily segment interesting areas in the images. In Section 2, an integrated imaging system to obtain accurate and reproducible multi-spectral images is proposed. The well defined and diffuse illumination of the optically closed scene aims to avoid shadows and specular reflections. Furthermore, the system has been developed to guarantee the reproducibility of the collected images. This allows for comparative studies of time series of images. In order to segment the interesting structure of the images, a novel segmentation algorithm, the Histogram Pursuit, is presented in Section 3. This algorithm combines the information provided by all the different spectral bands to enhance the main structures of the image. The performance of both the equipment and the Histogram Pursuit algorithm to achieve the above commented goal is tested and shown in Section 4. The obtained results and extensions of the developed work are discussed in Section 5.

## 2. Collecting multi-spectral images

The acquisition of the multi-spectral images was conducted in collaboration with Videometer.<sup>1</sup> The proposed equipment, Videometer Lab, is composed of a camera, light emitting diodes and an integrating sphere. The equipment has been designed to produce completely diffuse light that avoid shadows and specular reflections. The system acquires the multi-spectral images by fast strobe illumination from light emitting diodes (LEDs) at up to 20 different wavelengths.

Fig. 2(a) shows the equipment. Fig. 2(b) displays a sketch of the set-up. It displays the position of the camera, the diodes inside of the sphere, and the place where the object is located. Fig. 3(a) displays the position of the diodes inside the equipment. The camera resolution is  $1380 \times 1035$  pixels. In order to increase the accuracy and reproducibility of the images a radiometric and a geometric calibration are conducted [17]. The radiometric calibration

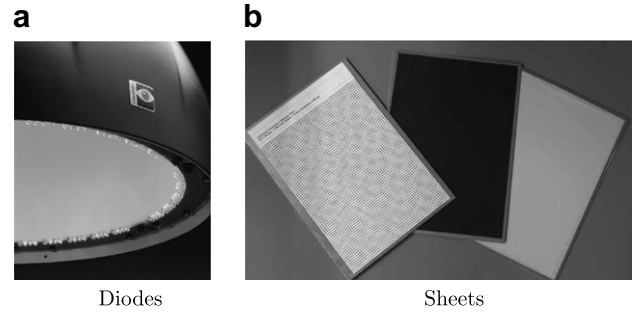


Fig. 3. Positioning of the diodes in the camera set-up and calibration sheets.

aims at eliminating problems with uneven intensities and vignetting, and to standardize the measurement scale. With this goal in mind two sheets of the natural color system (NCS) from the Scandinavian Color Institute were selected as calibration targets (NCS 1500 and NCS 8000). The equipment collects an image of each sheet. Then a non-linear calibration function is estimated and applied to each image pixel during the further image acquisition. The geometric calibration is conducted to make sure that aberrations, such as distortion, decentering and thin prism aberrations, do not affect the accuracy of the images. An image of a white sheet with black spots is grabbed with the camera for each wavelength. This calibration target is shown in Fig. 3(b), together with the radiometric sheets. The collected multi-spectral images are threshold and the center of gravity of each spot is calculated. A third order polynomial is applied to warp the centers of gravity to a given target. This is done for each band in the multi-spectral image in order to assure co-site registration.

## 3. The Histogram Pursuit (HP) algorithm

The core of the proposed segmentation algorithm is found in Friedman's Projection Pursuit algorithm [18]. Projection Pursuit (PP) is a statistical technique developed to find interesting structures in the data. Interesting structures are found via linear projections in which the distribution of the projected data differs as much as possible from the Gaussian distribution. Friedman justifies the non-interest of the normal distribution based on a series of properties as all the projections of a multivariate normal distribution are normal or that, for a fixed variance, the normal distribution has the least information (Fisher, negative entropy). The deviation from a Gaussian is measured through an index that measures the non-normality of the projected data.

In 1D, Friedman looks for a projection of the sphered data  $Z$ ,  $X = \alpha^T Z$ , such that the index

$$I(\alpha) = \frac{1}{2} \sum_{j=1}^J (2j+1) \left[ \frac{1}{N} \sum_{i=1}^n P_j(2\Phi(\alpha^T z_i) - 1) \right]^2,$$

is maximized.  $P_j$  is the Legendre polynomial of order  $j$  and  $\Phi(X)$  is the standard normal density function.

<sup>1</sup> [www.videometer.com](http://www.videometer.com).

Once an interesting projection has been found, the information obtained by this projection is removed and the algorithm looks for the next informative view. This process consists of transforming the data so that the density of the transformed data  $Z^{k+1}$  is as close as possible to the old data  $Z^k$  under the constraint that its marginal density is normal. This produces the closest distribution in the sense of the relative entropy distance measure

$$\int \log(Z^k / Z^{k+1}) Z^k dZ.$$

As it can be observed in Fig. 4(b), Friedman’s algorithm finds a projection that separates the two populations embedded in the synthetic dataset analyzed previously with PCA. This indicates that, from a classification point of view, maximizing the non-gaussianity of the projected data is a more appropriate criterion than to maximize the variance. However, maximizing the non-gaussianity of the projected data is too general. This may in datasets with more than two classes, or datasets that have some non-gaussian variables, e.g., uniform variables, result in the projection found by PP to be not optimal and thereby require more than just one projection. This would cause the computational inconvenience of having to analyze each projection found in order to discover the combination that enhances the desired structure. This fact is illustrated in Fig. 4. Fig. 4(e) shows the histogram of the data projected on the first projection obtained by PP of the dataset illustrated in Fig. 4(d). This dataset is composed of three Gaussian populations with 5000 data points each, means [10–1], [1015] and [2215], and covariance matrices:

$$\begin{pmatrix} 9 & 0 \\ 0 & 9 \end{pmatrix}, \begin{pmatrix} 6 & 0 \\ 0 & 6 \end{pmatrix} \text{ and } \begin{pmatrix} 4 & 0 \\ 0 & 4 \end{pmatrix}.$$

Note, that the first projection found by PP discriminates one of the populations with respect to the others. If the desired structure is not discriminated, then a second projection must be obtained in order to discriminate the wanted structure. However, there exists a one-dimensional projection that separates all of the three populations.

In order to find this combination, the proposed algorithm modifies Friedman’s index in order to incorporate information about the number of structures included in the image. If the image to be analyzed is assumed to have  $n$  classes, the index associated to a specific projection is defined as the  $n - 1$  largest area between two consecutive modes in the histogram of the projected data. The region where the HP algorithm calculates its index is illustrated in Fig. 5. The region is labeled Area. If  $M_{\min}$  represents the minimum histogram value calculated in the two maximums that define the area ( $x$  and  $y$ ),  $n_{\text{bins}}$  is the number of bins between these two maximums, and  $H(i)$  is the value of the  $i$ th bin, then the index is calculated by:

$$I(\lambda) = \left( \sum_{i=x}^{i=y} \min(H(i), M_{\min}) \right) - M_{\min} \times n_{\text{bins}}.$$

Notice that this index is scale invariant. If the found combination is  $\sum_i^{n_{\text{bands}}} \alpha_i B_i$ , then the combination  $\beta(\sum_i^{n_{\text{bands}}} \alpha_i B_i)$ ,  $\beta \in \mathfrak{R}$ , has the same index. In order to force the algorithm to provide only projections with  $n$  modes, the

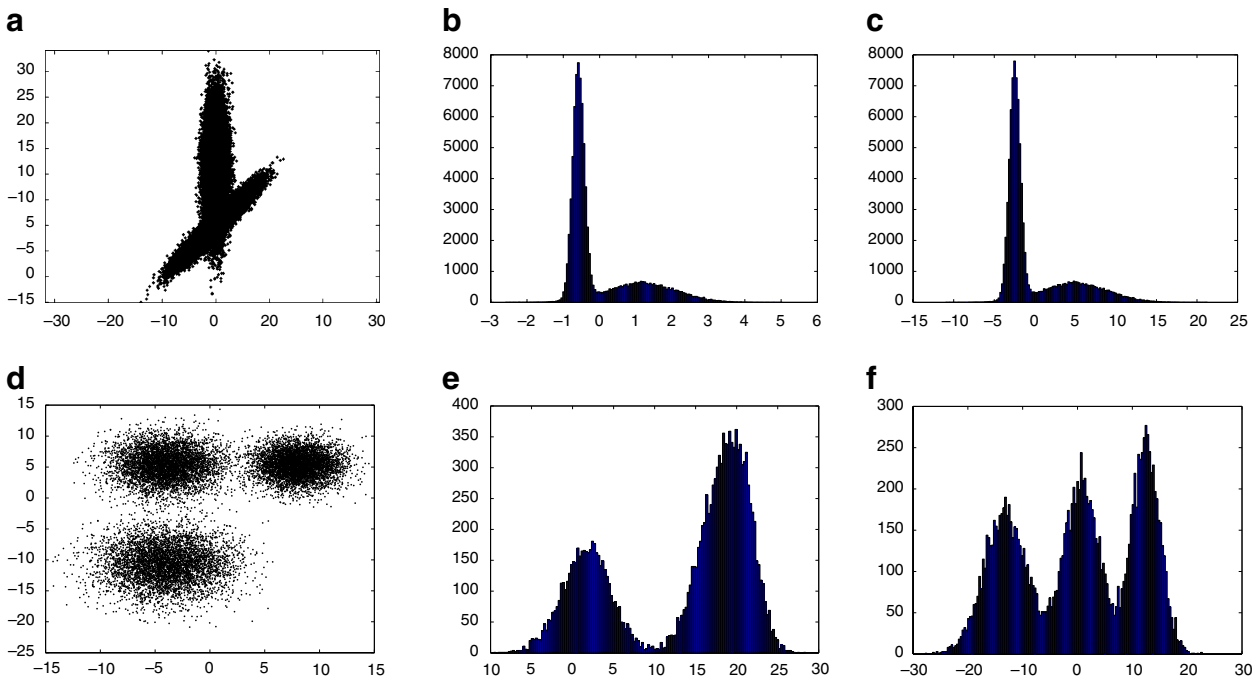


Fig. 4. Top row: (a) A two-dimensional dataset composed of two Gaussian populations. (b) Histogram of the projected data obtained using the combination found by PP. (c) Histogram of the projected data obtained using the combination found by HP. Bottom row: (d) A three-dimensional dataset composed of three Gaussian populations. (e) Histogram of the projected data obtained using the combination found by PP. (f) Histogram of the projected data obtained using the combination found by HP.

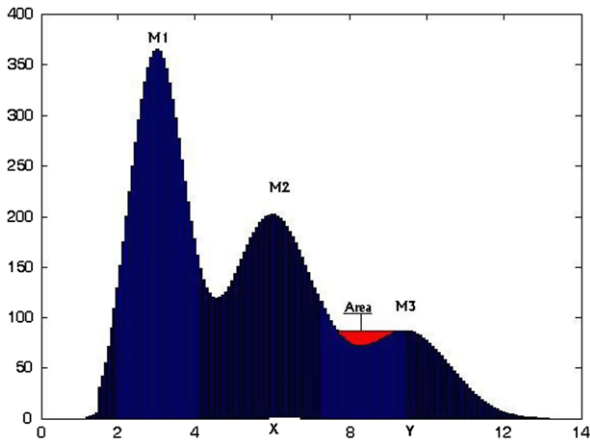


Fig. 5. Region where HP calculates the index.

Table 1  
Pseudo-code for HP index

---

Let  $H$  be an obtained histogram, and  $n$  the number of classes in the image

- 1-Smooth  $H$  to remove insignificant maxima
- 2-Detect all the local maxima of the smoothed histogram. Set  $n_{\max}$  to the desired number of maximums in  $H$
- 3-If  $n_{\max}$  is equal to  $n$  then
  - 3.a-FOR  $i$  equal 1 to  $n-1$  find the area between maximum  $i$  and maximum  $i+1$
  - 3.b-Index equal to the  $n-1$  largest area

Else  
Index = 0

Return Index

---

algorithm gives an index of zero to all projections with a number of modes different to  $n$ . A pseudo-code to calculate the index is given in Table 1.

The optimization in this work is conducted using genetic optimization [19].

#### 4. Experimental results

In this section, three experiments are conducted to test the accuracy and applicability of the proposed equipment and segmentation techniques. The first experiment aims to show the accuracy and reproducibility of the obtained images. The last two experiments show the results obtained by the segmentation technique in two different databases: a dermatological and a mycology database.

##### 4.1. Experiment 1: Testing the performance of the VideometerLab to collect reproducible and accurate images

The first experiment aims at demonstrating the accuracy of the system and the reproducibility of the acquired images. Reproducibility means that if the same image is collected at different times, the results should be comparable. This fact is really important when the objective is to detect and evaluate changes in bitemporal images. It guarantees that the

differences in two images taken some time apart do not depend on the conditions under which they have been taken. For instance, this quality is of prime importance in applications such as evaluation of dermatological lesions where it is important to ensure that differences in the obtained measures depend only of changes in the lesion.

In order to assess the reproducibility of the images, the equipment was kept turned on during 7 h. The set-up was calibrated every hour and images of four Natural Color System sheets (1500 N, 2500 N, 5000 N and 8500 N) from Scandinavian Color Institute were collected. The NCS sheets are all painted and have very small variation. The mean of each spectral band of the collected images was calculated. If the system performs accurately, the mean should not vary significant with respect to time. Marks were placed in the NCS sheets to calculate the mean in approximately the same area.

Fig. 6 shows the evolution of the measures with respect to time of the four NCS sheets in the amber band (592 nm). Results obtained in the other bands are similar to that obtained in this band. From the figure, it is noticed that the variation is minimal. After the first hour, where the equipment reached thermal equilibrium, the differences are inappreciable. Moreover, for fixed NCS sheet, the variance of the obtained measurements for each band is minimal.

In Table 2, the variance of the measurements obtained for each band of the different NCS sheets is displayed. This small variance guarantees that measures obtained in the image depend only on the structure being analyzed and it shows the robustness of the equipment.

##### 4.2. Experiment 2: Segmenting 9 multi-spectral band psoriasis images

The goal of the second experiment is to assess the use of multi-spectral images when analyzing dermatological

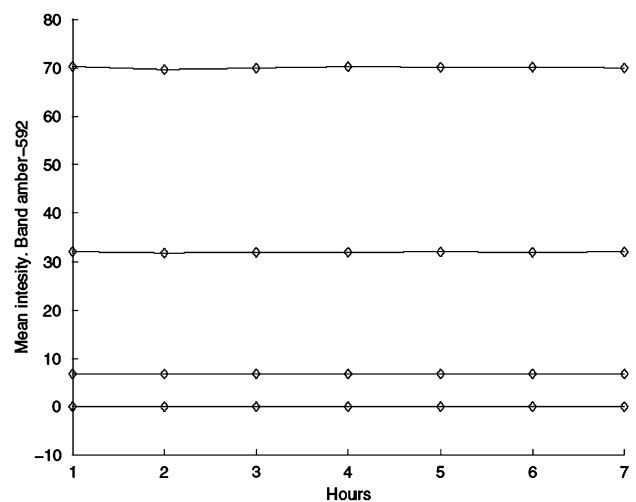


Fig. 6. Variation in the measurements of the NCS respect to the time that the equipment was turned on in the amber band, 592 nm.

Table 2  
Variance of the seven means obtained for each NCS sheet in each spectral band

Band/NCS number	1500 N	2500 N	5000 N	8500 N
Blue 472	0.0007	0.0105	0.0236	0.0348
Green 515	0.0002	0.0012	0.0028	0.0074
Amber 592	0.0013	0.0371	0.1295	0.1563
Red 630	0.0012	0.0078	0.0199	0.0222
Near IR 875	0.0010	0.0062	0.0434	0.0366
Ultra blue 428	0.0058	0.0057	0.0141	0.0320
Cyan 503	0.0003	0.0011	0.0023	0.0086
Orange 612	0.0004	0.0066	0.0234	0.0319
Near IR 940	0.0001	0.0076	0.0501	0.0726

lesions. Nowadays, the medical tracking of dermatological diseases is imprecise. The main reason is the lack of suitable objective methods to evaluate the lesions. Presently, the severity of the disease is scored by doctors just through their visual examination. Doctors visually assess the lesion and make scorings and journal notes of the current condition. These notes and perhaps some photographs are usually the only memory of what the lesion looked like at the corresponding visit. Image analysts have tried to provide different solutions to these problems during the last decades [20–24]. However, difficulties in correctly acquiring the images [16], the limited information provided by the trichromatic images and the presence of artifacts such as hair [25] cause that precise and objective scores of the severity of the lesions cannot be obtained. In order to evaluate the benefits of using multi-spectral images, a collection of eight multi-spectral psoriasis images were collected in collabora-

tion with the dermatological department of Gentofte Hospital in Denmark. These multi-spectral images were composed of nine spectral bands ranging from 472 nm to 940 nm.

The nine bands of one of the collected images together with their associated wavelengths are displayed in Fig. 7. It is seen that one of the bands mainly shows the hair and the veins (630 nm). This situation was also observed in the other psoriasis images which presented these two structures (Fig. 8(a) and (b)). This fact indicates that the multi-spectral images provided a more informative representation of the lesion than the traditional RGB images. This extra information can be used to obtain a more precise evaluation of the lesion where hair and veins are removed.

In order to statistically assess the information provided by the extra bands, the images were segmented using the HP algorithm. The HP algorithm found a projection where the lesion exhibited a considerable contrast with respect to the other structures involved in the image (Fig. 8(c)). The data in these projections are distributed approximately according to a mixture of two Gaussians. The parameters of this model can be estimated [26] and the lesion extracted via discriminant analysis. Results of the segmentation are shown in Fig. 8(d). It is observed that the nine multi-spectral bands provide enough information to precisely separate the lesion from the other parts of the images. The segmented images were used to assess the information provided by the extra bands in terms of Mahalanobis distances between classes. Given two classes  $X$  and  $Y$  with observations  $X_1, \dots, X_{n_1}$  belonging to  $X$  and observations

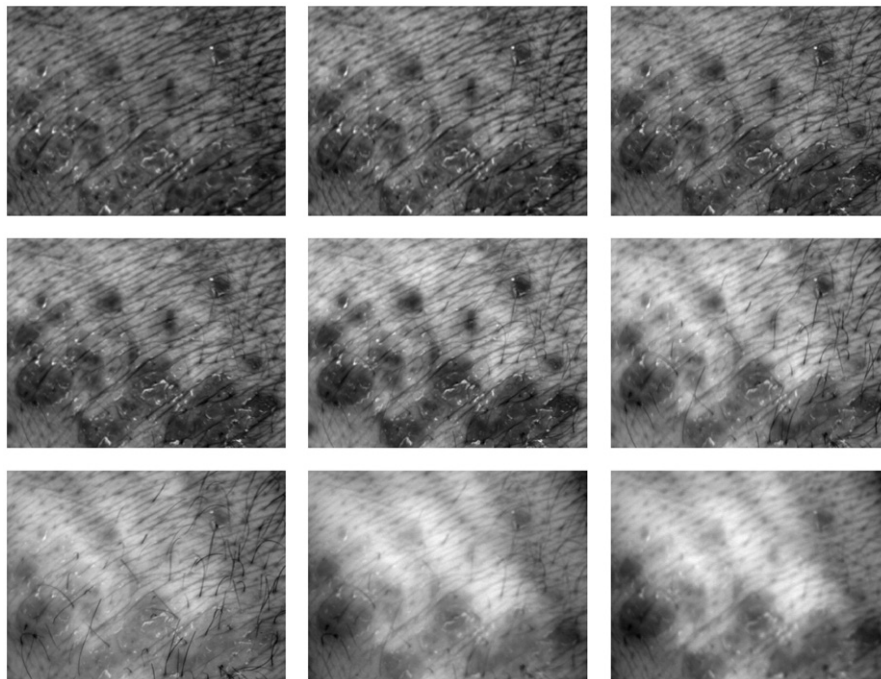


Fig. 7. The nine multi-spectral bands of one of the images. Top left: ultra-blue, 428. Top center: blue, 472. Top right: cyan, 503. Middle left: green, 515. Middle center: amber, 592. Middle right: orange, 612. Bottom left: red, 630. Bottom center: near infrared 875. Bottom right: near infrared 940. (For interpretation of the references to color in this figure legend, the reader is referred to the web version of this paper.)

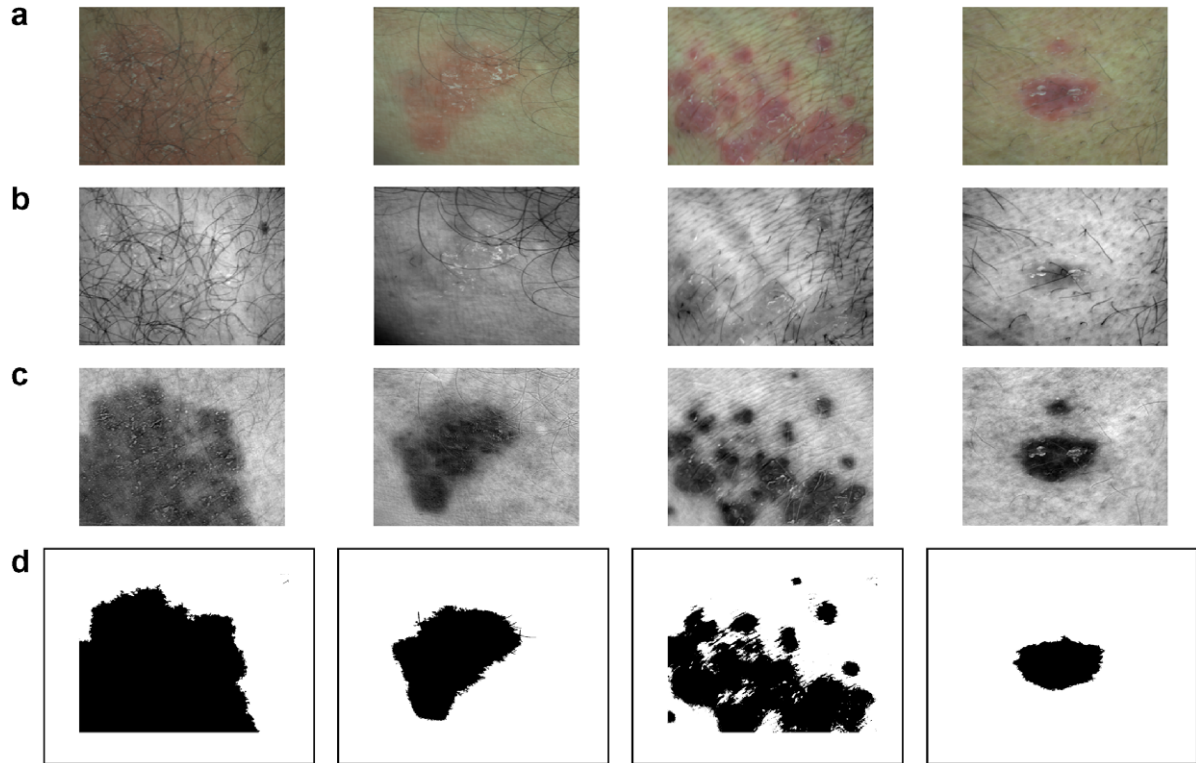


Fig. 8. (a) Four psoriasis images. (b) Spectral band 630 nm. (c) Projection image found by the HP algorithm. (d) Lesion segmentation.

$Y_1, \dots, Y_{n_2}$  belonging to  $Y$ , Mahalanobis distance between  $X$  and  $Y$  is defined by

$$(\mu_1 - \mu_2)^T \Sigma^{-1} (\mu_1 - \mu_2),$$

where  $\mu_1$  and  $\mu_2$  are the mean of classes  $X$  and  $Y$  respectively, and  $\Sigma$  is defined by

$$\Sigma = \frac{1}{n_1 + n_2 - 2} \left( \sum_i (X_i - \bar{X})(X_i - \bar{X})^T + \sum_i (Y_i - \bar{Y})(Y_i - \bar{Y})^T \right).$$

The Mahalanobis distances, for each of the eight images, between the lesion and the class composed of the other structures in the image (healthy skin, hair, ...) using the nine bands and using only a RGB approximation are shown in Table 3. It can be observed that the distance

Table 3  
Mahalanobis distances between the lesion and the other structures involved in the image

Image	Mahalanobis distance using the RGB bands	Mahalanobis distance using the nine bands
1	10.0793	12.8460
2	2.9048	10.3904
3	7.3857	12.2284
4	14.8222	17.4322
5	1.8920	23.4698
6	23.4068	38.4291
7	7.1864	9.9264
8	18.0009	31.8217

increases considerably when the nine bands are used. However, a more meaningful measure based on these measures is to statistically test the null hypothesis that the six extra bands does not contribute to a better discrimination. Specifically, if the extra six variables do not contribute to a better discrimination, then

$$Z = \frac{n_1 + n_2 - p - 1}{q} \frac{n_1 n_2 (D_p - D_q)}{(n_1 + n_2)(n_1 + n_2 - 2) + n_1 n_2 D_q},$$

follows a  $F(q, n_1 + n_2 - p - 1)$  distribution, where  $n_1$  and  $n_2$  are the number of observations on each class,  $p$  is the total number of variables,  $q$  is the number of variables that are to be tested if they do or do not contribute to a better discrimination and  $D_p$  and  $D_q$  are the Mahalanobis distances between classes using all the variables except the last  $q$ . Results showed that statistically the null hypothesis was rejected with a significance level of 1%. This means that the last six variables strongly contribute to a better discrimination.

#### 4.3. Experiment 3: Segmenting 18 multi-spectral band fungi images

Classification of fungi is of importance for several reasons; for a further phylogenetic study or to reveal new species or isolates to use in, e.g., food or medical industries.

Traditionally, the classification has been performed by means of chemical and visual studies of the fungi. In the last decade digital image analysis has also been utilized

for the classification, but till now it has been based on RGB images as in [27].

The species can be differentiated by macroscopic features, microscopic features and behaviors like, e.g., thermophilicity (whether or not they can grow at high temperatures). The macroscopic features are the ones captured by the image acquisition.

The *Penicillium* genus was chosen due to the large knowledge of and well identified isolates. *Penicillium* is a filamentous fungi also known as mold. Most of the species are found in the soil and in the air. They are known to produce mycotoxins. The mycotoxins can cause infections when in contact with humans, though, depending of the type of mycotoxin. The fungi can also be used to produce antibiotics, antitoxins and other drugs.

Multi-spectral images with 18 wavelengths are examined. Three species are examined: *P. polonicum*, *P. venetum*, and *P. melanoconidium*. It is assumed that the many spectra additionally can reveal some chemical information about the fungi compared to the ordinary RGB images. Within each species four different isolates were chosen, all obtained from the IBT Culture Collection held at BioCentrum-DTU. They were chosen with geographical origin in different countries to get a greater variance within each specie. Each isolate was grown on three different media: OAT (Oatmeal Agar), YES (Yeast Extract Sucrose Agar), and CYA (Czapek Yeast Extract Agar), with three replicas on each medium to obtain the variance within each isolate. The isolates are grown on three media to get access to more information. This is the usual prac-

tice when isolates are to be identified. In total there are 108 samples.

The first step is to segment the background, the petri dish and the fungi into three classes. The next step is to examine each of the three classes and then respectively examine each of the subclasses obtained for further classes until a subclass no longer can be split in two or more. The interest is to segment the fungi from the background as well as the petri dish, and if possible extract information of differences within the fungi. This is done in order to extract features to be used in a further classification of the species. The first step is straight forward in all cases where as the following examinations differ depending on the appearance of the individuals.

#### 4.3.1. Results of the segmentation

Fig. 9 shows examples of segmentations within the images of the three species grown on the YES medium. The fungi are well separated from both petri dish and background, and furthermore, the lighter edge of the fungi can be separated from the darker center of the fungi. The latter can be useful since the different species differ in appearance at this point. The images are foremost split into 3 classes: The background, the medium, and the fungi. As this is not sufficient the medium and the fungi classes are further examined for subclasses. Subdividing further, the lighter edge is separated from the medium class and small segments of the medium is separated from the fungi class.

Fig. 10 illustrates two examples on the OAT medium where the lighter edge of the fungi are segmented from the

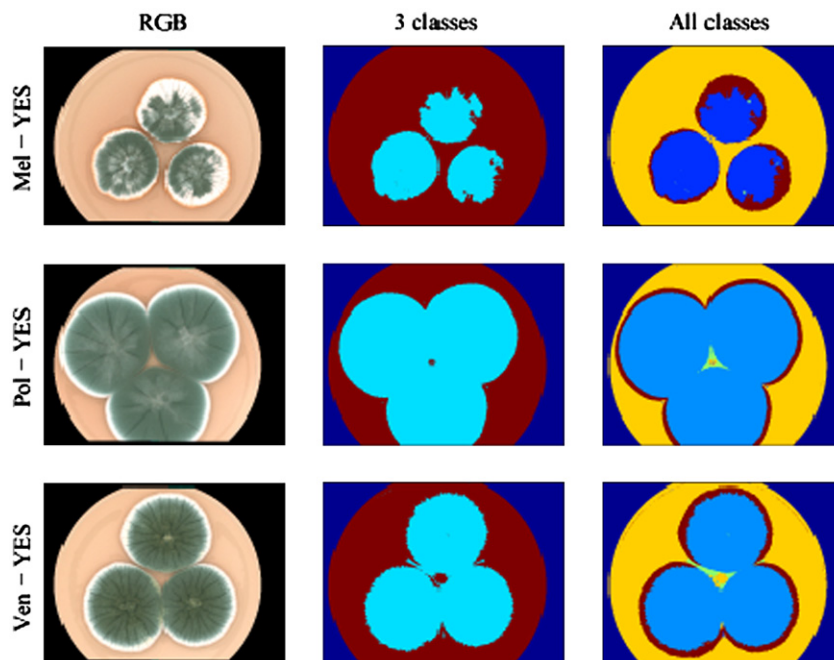


Fig. 9. Segmentation of a *P. melanoconidium*, a *P. polonicum*, and a *P. venetum* isolates all on the YES medium with IBT numbers: 3445, 22439 and 21549, respectively. First column illustrates RGB representations of the multi-spectral images. Second column illustrates the first segmentation in to three classes. The third column illustrates the final segmentation.

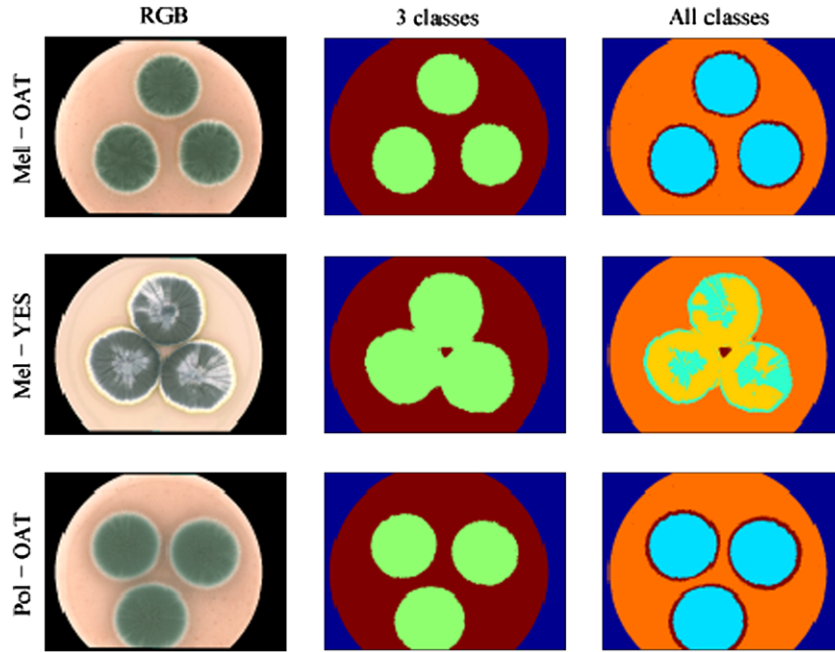


Fig. 10. Segmentation of a *P. polonicum*, and two *P. melanoconidium* isolates on the OAT and YES media with IBT numbers: 22439, 3445 and 10031, respectively. First column illustrates RGB representations of the multi-spectral images. Second column illustrates the first segmentation in to three classes. The third column illustrates the final segmentation.

medium classes. Another example of a *P. melanoconidium* on YES medium is shown. In this case the lighter areas of the fungi are classified as fungi first time, but partitioning further gives a subdivision of the fungi area.

In Fig. 11 the division of the segmented medium was performed using three classes. For the *P. venetum* isolate

in the middle row the segmented fungi was divided further as it contained some of the medium. The edge of the fungi was not identified when first dividing the segmented medium, but at the following segmentation. The divisions of the media may be useful for examinations of the chemicals the fungi produce during the growth.

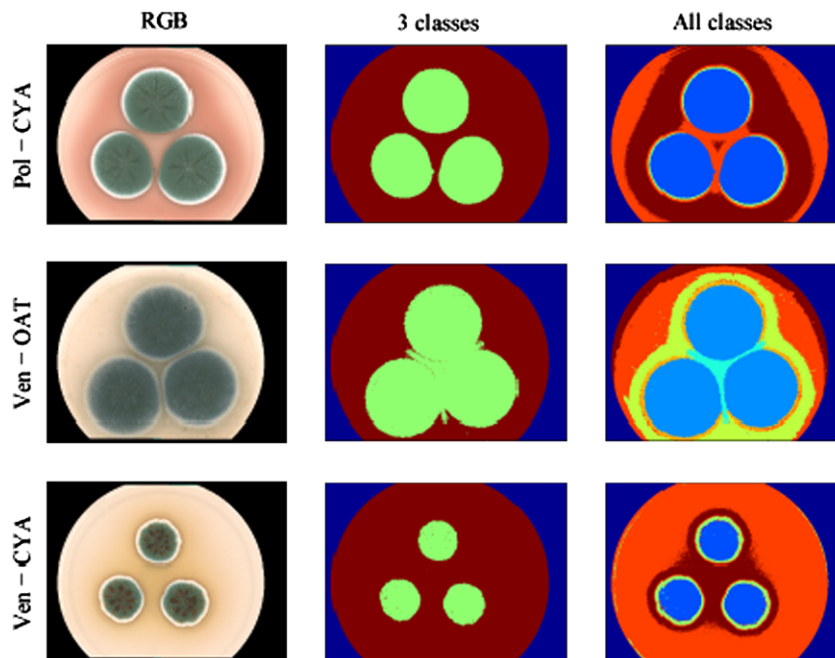


Fig. 11. Segmentation of a *P. polonicum* and two *P. venetum* isolates all on the CYA and OAT media with IBT number: 15982, 23039 and 16215, respectively. First column illustrates RGB representations of the multi-spectral images. Second column illustrates the first segmentation in to three classes. The third column illustrates the final segmentation.

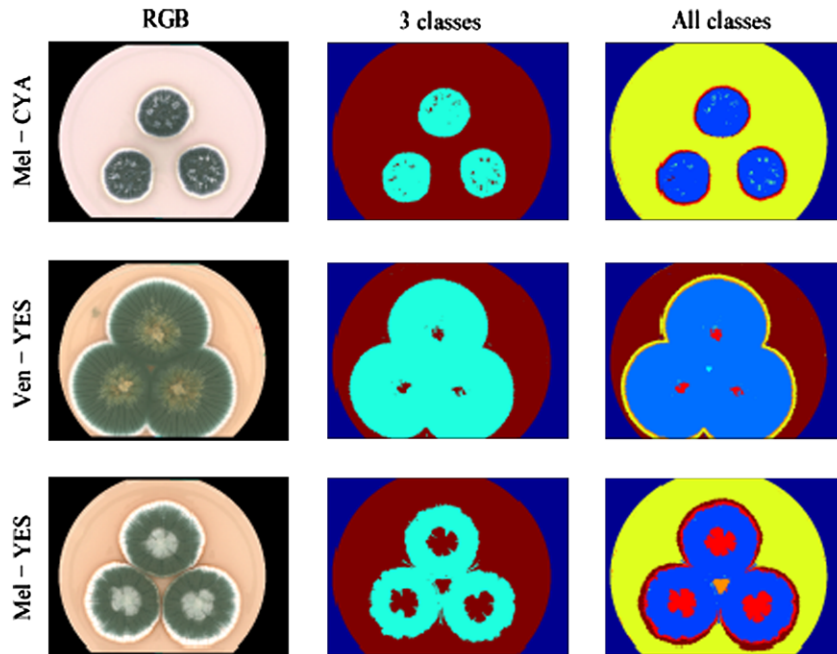


Fig. 12. Segmentation of a *P. melanoconidium* and two *P. venetum* isolates all on the CYA and YES media with the IBT numbers: 21534, 23039 and 21534, respectively. First column illustrates RGB representations of the multi spectral images. Second column illustrates the first segmentation in to three classes. The third column illustrates the final segmentation where each of the three classes first found are examined for further divisions.

Fig. 12 illustrates isolates where the fungi can be divided into more subgroups than two; the edge and the center of the fungi. Two *P. melanoconidium* isolates and one *P. venetum* isolate are shown on the CYA and YES media.

Segmentations of multi-spectral images of the three *Penicillium* species on the three different media have been conducted. Examples from each group have been illustrated. There are three examples where the appearance of the fungi have some variance within the 9 groups and these are also illustrated. The results shown illustrate that the fungi are well separated from the media for different isolates. Furthermore, the method can be used to find subclasses within the fungi.

## 5. Conclusions

In this work, a system to collect precise and reproducible multi-spectral dermatological images has been proposed. The system can collect up to 20 different spectral bands. These bands are composed by the RGB tri-chromatic spectral bands plus 17 extra bands that can be chosen in the range going from ultra-blue to near infrared (from 395 nm to 970 nm). The reproducibility of the equipment has been tested. A novel algorithm that combines the information of all the spectral bands in order to segment the interesting areas have also been provided. Results indicate that the equipment and the segmentation algorithm are suitable tools to measure changes in the evolution of dermatological disease. Furthermore, it has been observed that the six extra bands provide more information than the classical RGB images. This information can be used to remove noise such as hair or occlu-

sions and to obtain more precise measures to characterize the lesion. Furthermore, the applicability of the equipment and the segmentation algorithm was tested on a second data base of fungi images. It was shown that fungi as well as some structures in the fungi can be segmented to obtain features for further classification. Results point out the proposed imaging system as a suitable tool for obtaining measures that characterize the objects under study.

## Acknowledgments

The authors would like to thank to the SITE Project funded by a grant from the Danish Technical Research Foundation (Project Number STVF 56-00-0123) for supporting the present work. The authors would also like to thank the dermatologists Lone Skov and Bo Bang of Gentofte Hospital of Denmark and the anonymous patients, for their collaboration during the image acquisition. The authors also thank Jens Christian Frisvad from Biocentrum department at the Technical University of Denmark for providing the fungi samples.

## References

- [1] G. Wyszecky, W. Stiles, Color Science: Concepts and Methods, Quantitative Data and Formulae, Wiley, New York, 1982.
- [2] H. Ganster, A. Pinz, R. Rohrer, E. Wildling, M. Binder, H. Kittler, Automated melanoma recognition, IEEE Transactions on Medical Imaging 20 (3) (2001) 233–239.
- [3] G. Hance, S. Umbaugh, R. Moss, W. Stoecker, Unsupervised color image segmentation, with application to skin tumor border, IEEE Engineering in Medicine and Biology 15 (1) (1996) 104–111.

- [4] C. Garcia, G. Tziritas, Face detection using quantized skincolor regions merging and wavelet packet analysis, *IEEE Transactions on Multimedia* 1 (3) (1999) 264–277.
- [5] S.L. Phung, A. Bouzerdoum, D. Chai, Skin segmentation using color pixel classification: analysis and comparison, *IEEE Transactions on Pattern Analysis and Machine Intelligence* 27 (1) (2005) 148–154.
- [6] C.J. Du, D.W. Sun, Comparison of three methods for classification of pizza topping using different colour space transformations, *Journal of Food Engineering* 68 (3) (2005) 277–287.
- [7] A. Ihlow, U. Seiffert, Automating microscope colour image analysis using the expectation maximisation algorithm, proceedings of the 26th DAGM Symposium in Pattern Recognition, Springer Verlag, Berlin, 2004.
- [8] G. Luo, O. Chutatape, H. Li, S. Krishnan, Abnormality detection in automated mass screening system of diabetic retinopathy, *Proceedings 14th IEEE Symposium on Computer-Based Medical Systems* (2001) 132–137.
- [9] X. Zhang, O. Chutatape, Detection and classification of bright lesions in color fundus images, 2004 International Conference on Image Processing 1 (2004) 139–142.
- [10] I.T. Jolliffe, *Principal Component Analysis*, Springer Series in Statistics, 2002.
- [11] M.A. Turk, A.P. Pentland, Face recognition using eigenfaces, *Proceedings CVPR 1991* (1991) 586–591.
- [12] R. Duda, P. Hart, *Pattern Classification and Scene Analysis*, Wiley, New York, 1973.
- [13] M. Vhrel, H. Trussell, Color device calibration: A mathematical formulation, *IEEE Transactions on Image Processing* 8 (1999) 1796–1806.
- [14] Y. Vander, Y. Haeghen, J.M. Naeyaert, I. Lemahieu, An imaging system with calibrated color image acquisition for use in dermatology, *IEEE Transactions on Medical Imaging* 19 (7) (2000) 722–730.
- [15] I. Maglogiannis, Design and implementation of a calibrated store and forward imaging system for teledermatology, *Journal of Medical Systems* 28 (5) (2004) 455–467.
- [16] A. Gutenev, V.N. Skladnev, D. Varvel, Acquisition-time image quality control in digital dermatoscopy of skin lesions, *Computerized Medical Imaging and Graphics* 25 (2001) 495–499.
- [17] J. Folm-Hansen, *On Chromatic and Geometrical Calibration*, Ph.D. thesis, Technical University of Denmark, 1999.
- [18] J. Friedman, J. Tukey, A projection pursuit algorithm for exploratory data analysis, *IEEE Transactions on Computers* 23 (9) (1974) 881–889.
- [19] D.E. Goldberg, *Genetic Algorithms in Search, Optimization, and Machine Learning*, Addison Wesley, Reading, MA, 1989.
- [20] P. Schmid-Saugeon, J. Guillod, J.P. Thiran, Towards a computer-aided diagnosis system for pigmented skin lesions, *Computerized Medical Imaging and Graphics* 27 (2003) 65–78.
- [21] M. Nischik, C. Forster, Analysis of skin erythema using true-color images, *IEEE Transactions on Medical Imaging* 16 (6) (1997) 711–716.
- [22] M. Hintz-Madsen, L.K. Hansen, J. Larsen, K.T. Drzewiecki, A probabilistic neural network framework for detection of malignant melanoma, in: R. Naguib, G. Sherbet (Eds.), *Artificial Neural Networks in Cancer Diagnosis, Prognosis and Patient Management*, Vol. 5, CRC Press, Boca Raton, FL, 2001, pp. 3262–3266.
- [23] P. Schmid, Segmentation of digitized dermatoscopic images by two-dimensional color clustering, *IEEE Transactions on Medical Imaging* 18 (2) (1999) 165–171.
- [24] N. Engstrom, F. Hansson, L. Hellgren, J. Tomas, B. Nordin, F. Vincent, A. Wahlberg, Computerized wound image analysis, *Pathogenesis of Wound and Biomaterial-Associated Infections* (1990) 189–193.
- [25] D.H. Chung, G. Sapiro, Segmenting skin lesions with partial-differential-equations-based image processing algorithms, *IEEE Transactions on Medical Imaging* 19 (7) (2000) 763–767.
- [26] T. Taxt, N.L. Hjort, L. Eikvil, Statistical classification using a linear mixture of two multinormal probability densities, *Pattern Recognition Letters* 12 (1991) 731–737.
- [27] M.E. Hansen, *Indexing and Analysis of Fungal Phenotypes Using Morphology and Spectrometry*, Ph.D. thesis, Technical University of Denmark, 2003.